ACS NANO

www.acsnano.org

ARTICLE

Ultrathin and Deformable Graphene Etch Mask for Fabrication of 3D Microstructures

Jiwoo Kim, Donghoon Moon, Hyunchul Kim, Arend M. van der Zande, and Gwan-Hyoung Lee*

Cite This: https://doi.org/10.1021/acsnano.4c01279

Read Online

ACCESS | Metrics & More | Article Recommendations | Supporting Information

ABSTRACT: Three-dimensional (3D) microfabrication techniques play a crucial role across various research fields. These techniques enable the creation of functional 3D structures on the microscale, unlocking possibilities for diverse applications. However, conventional fabrication methods have limits in producing complex 3D structures, which require numerous fabrication steps that increase the costs. Graphene is an atomically thin material known for its deformability and impermeability to small gases and molecules, including reactive gases like XeF_2. These features make graphene a potential candidate as an etch mask for 3D microfabrication. Here, we report the fabrication of various 3D microstructures using graphene etch masks directly grown and patterned on a Si substrate. The patterned graphene deforms and wraps the etched structures, allowing for the fabrication of complicated 3D microstructures, such as mushroom-like and step-like microstructures. As a practical demonstration of the graphene etch mask, we fabricate an omniphobic surface of reentrant 3D structures on a Si substrate. Our work provides a method for fabricating complex 3D microstructures using a graphene etch mask, contributing to advancements in etching and fabrication processes.

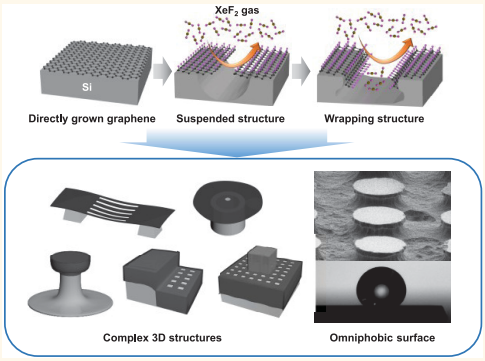

KEYWORDS: *3D microfabrication, graphene etch mask, etching selectivity, graphene wrapping, omniphobic surface*

INTRODUCTION

The demand for three-dimensional (3D) microfabrication techniques is steadily growing across various fields, such as microelectromechanical systems (MEMS),[1,2] bioengineering,[3−5] microelectronics,[6] microfluidics,[7] and photonics.[8−11] Advanced fabrication technology of 3D microstructures plays an essential role in broadening the range of available options for material selection and sample scale. While conventional lithographic approaches are effective for mass production and large-scale patterning, their capability to produce intricate 3D microstructures remains limited because these methods often involve complicated and time-consuming processes for sculpting such structures.

Atomically thin graphene, known for its extraordinary properties of low bending stiffness,[12] high mechanical strength,[13,14] deformability,[15,16] impermeability,[17,18] high etch resistance,[19] and chemical stability,[20] holds immense potential beyond its traditional role in electronic applications. Specifically, it has been reported that graphene has exceptional etching resistance to XeF_2 gas, which is renowned for its high selectivity toward silicon, leading to extensive applications in microcantilevers and micromachining devices.[21] Instead of being etched by XeF_2, graphene becomes fluorinated graphene (FG).[22−25] Consequently, graphene presents the potential to serve as an impermeable etch mask[26] and an etch stop.[27] A key unexplored question is whether the other features of deformability can be leveraged in combination with etch resistance to enhance capabilities.

In this work, we report a technique for fabricating complicated 3D microstructures by using graphene as a deformable etch mask. The graphene grown directly on a Si substrate by chemical vapor deposition (CVD) showed outstanding resistance to XeF_2 gas, which makes it an excellent choice for an etch mask material. Furthermore, the ultrathin and flexible nature of graphene allows it to conform to the underlying structures, enabling the production of intricate designs that previously necessitated complex procedures. Additionally, integrating a flexible graphene mask with various pattern designs facilitates the production of complex 3D structures with controlled etching depths. As an example of diverse applications, we fabricated omniphobic surfaces on a Si substrate with arrays of reentrant structures by using a deformable graphene etch mask.

Received: January 26, 2024
Revised: March 26, 2024
Accepted: April 22, 2024

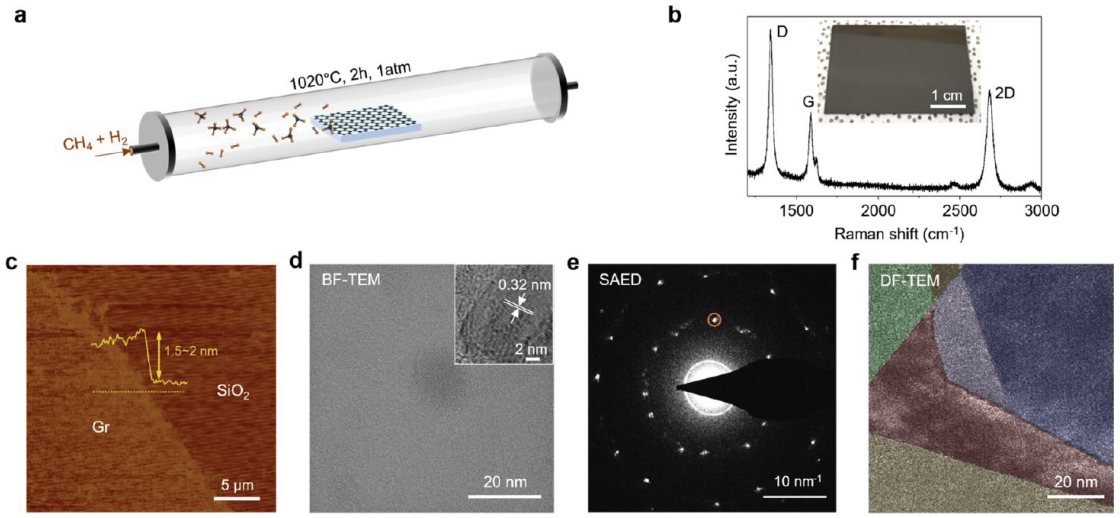

Figure 1. Direct growth of graphene on the Si substrate and characterization of the as-grown graphene. (a) Schematic depicting the direct growth of graphene on the Si substrate. (b) Raman spectrum of grown graphene. Inset: image of the large area of graphene grown on Si. (c) AFM height image of the grown graphene. (d) Bright-field TEM image. Inset: high-magnification high-resolution TEM (HRTEM) image. (e) Corresponding diffraction pattern of polycrystalline graphene in (d). (f) Dark-field TEM image with the orange circle in (e) corresponding to the selected aperture.

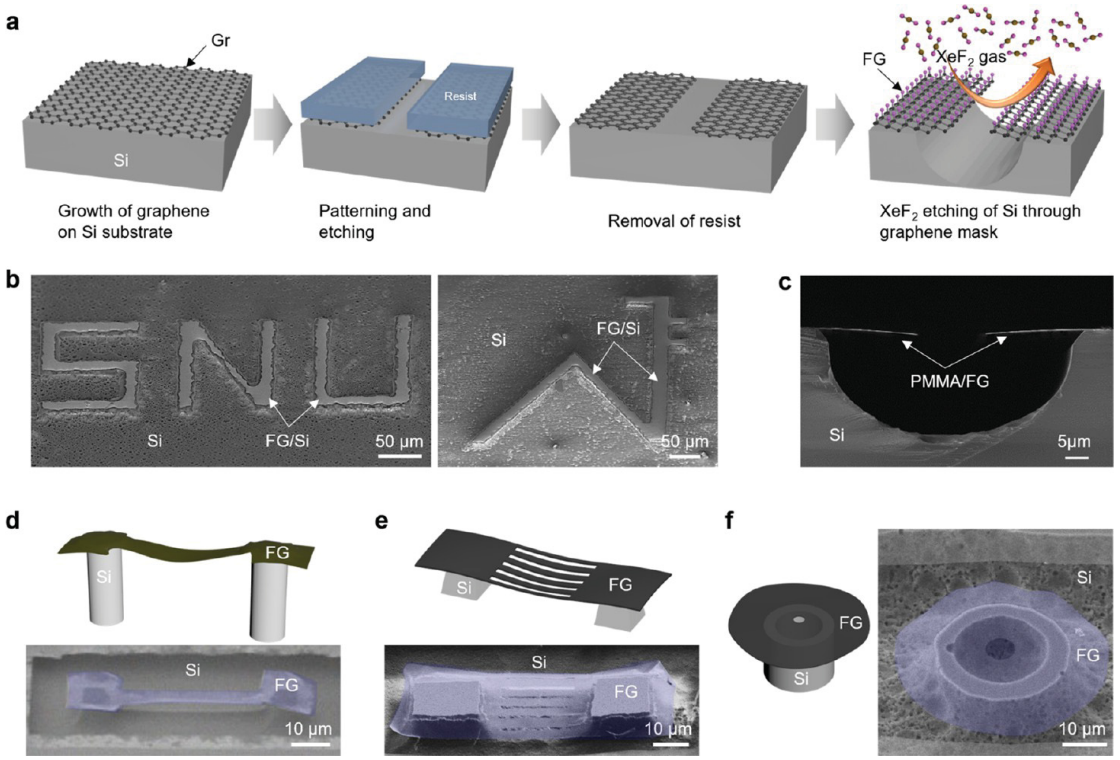

Figure 2. Fabrication of suspended structures with a graphene mask. (a) Schematic illustrating the fabrication process of the suspended structure on the Si substrate. (b) Scanning electron microscopy (SEM) images of the etched Si surface with a patterned graphene mask. (c) Schematic of a cross-sectional view of the Si surface with a patterned graphene mask with a hole. (d–f) SEM images of various 3D suspended graphene structures. (d) 3D suspended structure with a narrow bridge (e) 3D suspended structure with patterned holes. (f) 3D suspended structure featuring a void within the structure.

RESULTS AND DISCUSSION

To utilize graphene as an etch mask, we first directly synthesized it on a silicon substrate by atmospheric pressure chemical vapor deposition (APCVD; Figure 1a). This approach avoids critical issues of damage and polymer residue during the transfer of graphene grown on a catalytic metal substrate.[28] The full recipe is shown in Figure S1. As shown in Figure 1b, we performed structural analysis of graphene using Raman spectroscopy. The inset shows an optical image of the graphene grown on the Si substrate. The Raman spectrum of graphene clearly shows two main G (1590 cm^{-1}) and 2D (2682 cm^{-1}) modes along with D (1344 cm^{-1}) and D′ (1623

https://doi.org/10.1021/acsnano.4c01279
ACS Nano XXXX, XXX, XXX−XXX

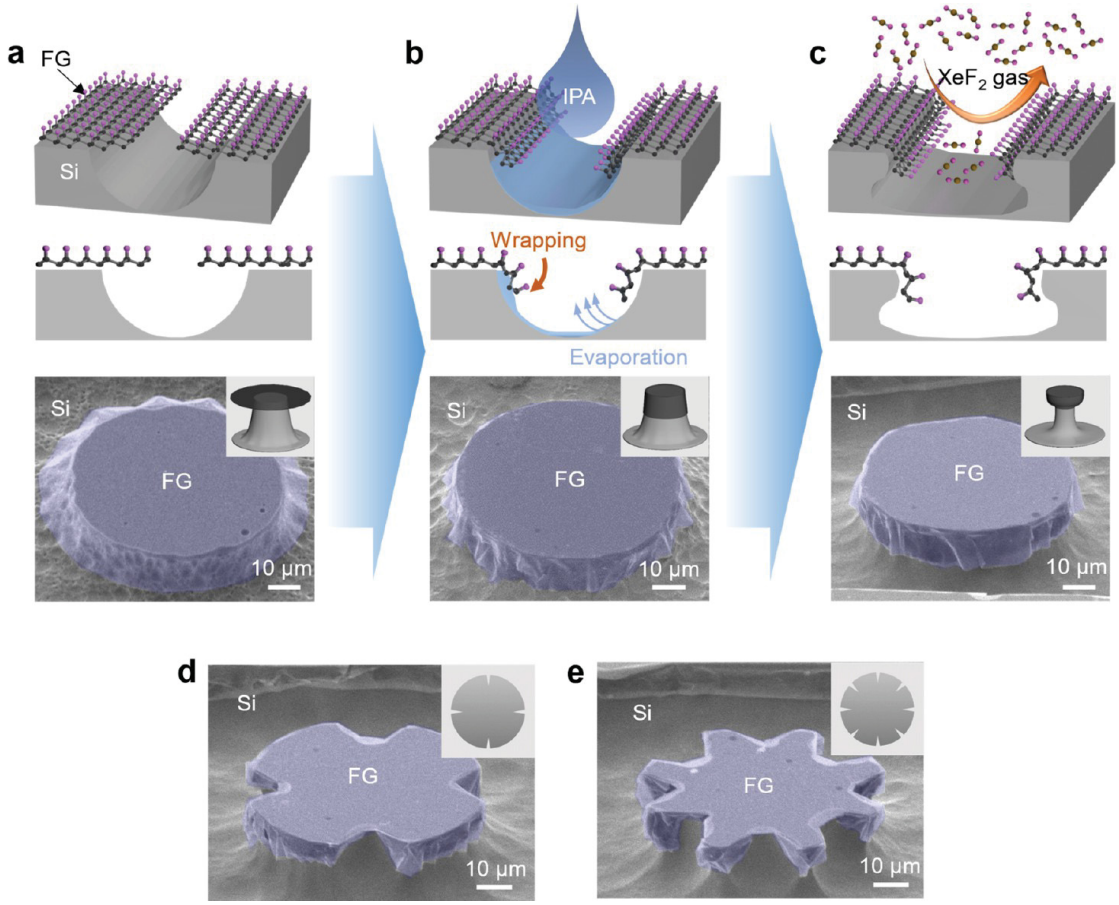

Figure 3. Fabrication of wrapping structures with a deformable graphene mask. (a–c) Schematic images and SEM images illustrating the fabrication process for wrapping structures. (d, e) Serrated reentrant structures fabricated through a wrapping and etching process using a deformable graphene mask. Inset: design of a graphene mask for each 3D structure.

cm^{-1}) modes. The well-defined G and 2D peaks show that graphene is crystalline. The presence of the high D peak indicates the significant presence of defects in the grown graphene, and the $I(D)/I(D')$ ratio of 4.3 suggests that the majority of these disorders are attributed to grain boundaries.[29] As shown in Figure 1c, we use atomic force microscopy (AFM) to confirm that the thickness of the grown graphene has a range of 1.5–2 nm, which corresponds to few-layer graphene of 4–5 layers. We investigated the crystal structure of the grown graphene using transmission electron microscopy (TEM, Figure 1d–f). The bright-field (BF) TEM image in Figure 1d shows that the graphene is smooth without patches or changes in thickness. The inset of Figure 1d is a higher magnification image showing the crystal structure. From this, we see that the lattice constant of the grown graphene is 0.32 nm, consistent with the theoretical value of pristine graphene. Figure 1e shows the selected area electron diffraction (SAED) pattern from the same location as the BF-TEM image of Figure 1d. The well-defined sets of spots with 6-fold symmetry indicate that the grown graphene is polycrystalline. The dark-field (DF) TEM image of Figure 1f, constructed from the diffraction spot of the orange circle in Figure 1e, shows that the grown graphene is polycrystalline with grain sizes of tens of nanometers and well-stitched grain boundaries.[30,31] Note that all grains are false-colored to show each grain.

Figure 2a schematically shows how we fabricate the graphene etch masks and use them to make suspended structures. We patterned the directly grown graphene on the Si substrate using e-beam lithography or photolithography and then etched the graphene into desired patterns using CF_4 plasma. After removal of the resist, the sample was exposed to XeF_2 gas to etch the Si substrate. Figure 2b shows an example of an etched 3D structure of the Seoul National University Logo. A key observation is that the regions of the silicon covered by the graphene etch mask exhibited no change.

In Figure 2c, we determine the etch rate of Si in vertical and lateral directions using a cross-sectional scanning electron microscopy (SEM) image of an 18 μm wide line in the graphene mask, exposed to XeF_2 gas at 3 Torr for a total of 200 s. The sample exhibits undercut etching under the mask, demonstrating a similar etch rate in both vertical and lateral directions, confirming isotropic etch characteristics of XeF_2. Additionally, the etching behavior of the Si substrate with the rectangularly patterned graphene mask exhibits isotropic etching in all in-plane directions (Figure S2a,b). The isotropic etching of XeF_2 results in undercut etching of the silicon substrate beneath the graphene mask, thus offering a technique to fabricate suspended 3D graphene/silicon structures.

In Figure 2d–f, we demonstrate how the undercut etching of Si beneath the graphene etch mask can be used to fabricate 3D suspended graphene structures. As shown in Figure 2d, during the XeF_2 etching process, the Si underneath the narrow graphene bridge was selectively etched, leaving behind Si supports beneath wider graphene patterns. This process led to

https://doi.org/10.1021/acsnano.4c01279
ACS Nano XXXX, XXX, XXX–XXX

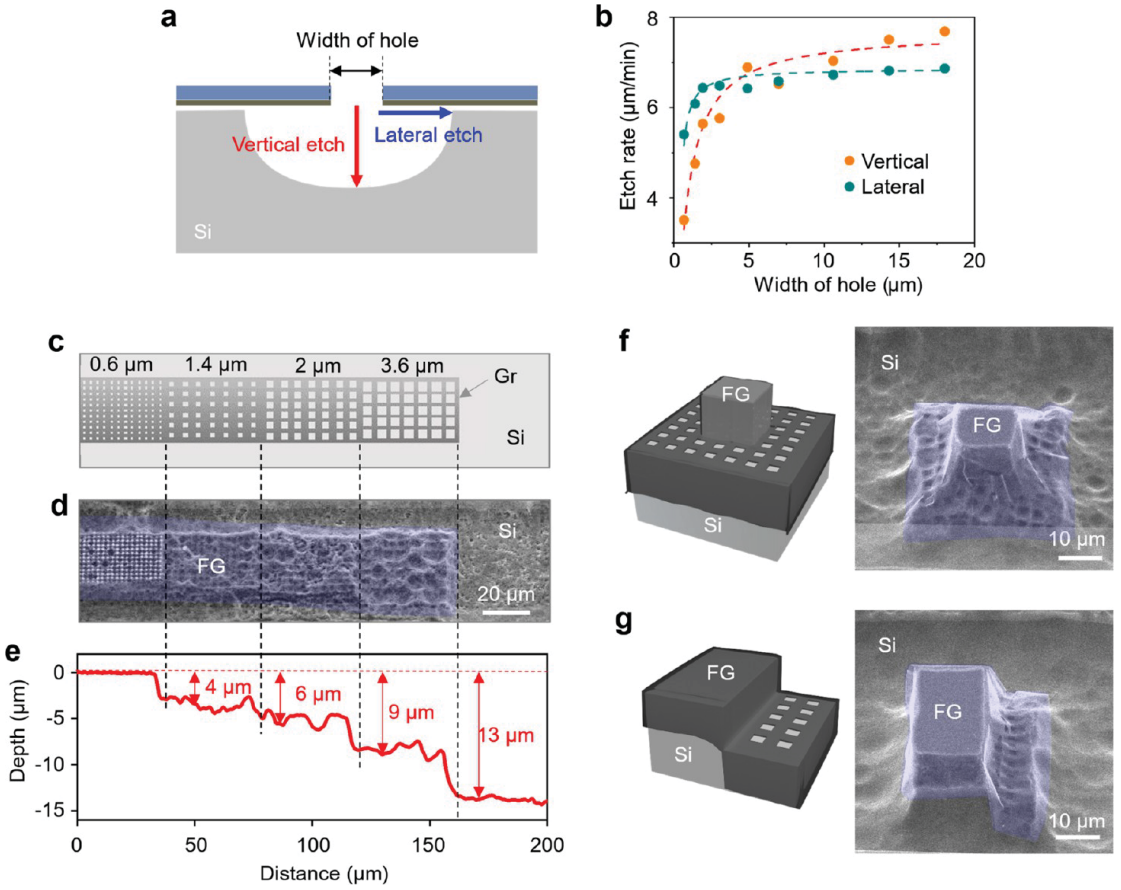

Figure 4. Controlling the etching depth in the fabrication of 3D structures. (a) A schematic of the cross-sectional view depicting the etched surface of a silicon substrate with a patterned mask. (b) The relationship between vertical and lateral etch rates on the hole width of the patterned graphene mask. (c–e) Control of etching depth depending on the size of holes in the graphene mask. (c) The design of a graphene mask featuring holes of different sizes at equal intervals. (d) SEM images of the etched surface with a graphene mask featuring holes of varying sizes. (e) Surface profiler measurement showing the etched silicon surface. (f, g) 3D structures fabricated by controlling the etching depth: (f) a protruding structure and (g) a step-like structure.

the formation of a suspended graphene bridge structure. Employing patterned perforations in the suspended bridge area proves to be an effective method for producing 3D suspended structures with a larger bridge surface area (Figure 2e). Unless these perforations in the bridge area are too small, they permit the silicon beneath the bridge region to undergo etching. Likewise, incorporating patterned perforations into the graphene mask design serves as a tactic for generating cavities within the silicon structure. By implementation of this approach, a 3D structure featuring graphene suspended on hollow, cylinder-shaped silicon was successfully fabricated (Figure 2f). By harnessing the isotropic properties of XeF_2 and employing specific pattern design techniques for the etch mask, a diverse range of 3D suspended graphene/silicon structures were effortlessly created (Figure S3). This demonstrates boundless potential for crafting distinctive 3D suspended structures.

In Figure 3, we explore how to wrap the suspended graphene etch masks onto the underlying etched surfaces to achieve complex 3D structures. Figure 3a–c schematically shows the wetting process we used to wrap the graphene, along with representative isometric SEM images of each step on a patterned mushroom 3D structure. We applied isopropyl alcohol (IPA) onto the substrate and then let it dry. IPA is known to leave little surface residue and is commonly used as a last cleaning step in processing. As droplets of IPA naturally evaporate, the surface tension pulls on the suspended graphene and causes the flexible graphene mask to conform to the underlying Si structures (Figure 3b). The graphene firmly attached to the Si structures serves as a protective barrier during subsequent etching by XeF_2, resulting in reentrant structures (Figure 3c). We note that this process is sensitive to the thickness of the grown graphene because bending stiffness and deformability are sensitive to the thickness. In Figures S4 and S5, we explore this thickness dependence and show that monolayer and bilayer samples are more easily conforming to the surface. Likewise, the 30 min-grown graphene thinner than that grown for 2 h by reducing the growth time shows similar results with monolayer and bilayer samples.

In Figure 3d,e, we additionally fabricated diverse 3D structures, including the serrated reentrant structures, by utilizing graphene masks with serrated contours. The thickness of the upper protruding part of these 3D reentrant structures can be controlled by adjusting the length of the undercut region of graphene before the wrapping process (Figure S6a). More undercut etching under the graphene mask before the IPA dropping process results in the fabrication of structures with thicker upper protruding parts, while less undercut leads to the thinner thickness of upper parts. (Figure S6b) With a deformable graphene mask, complex 3D structures that are

https://doi.org/10.1021/acsnano.4c01279
ACS Nano XXXX, XXX, XXX−XXX

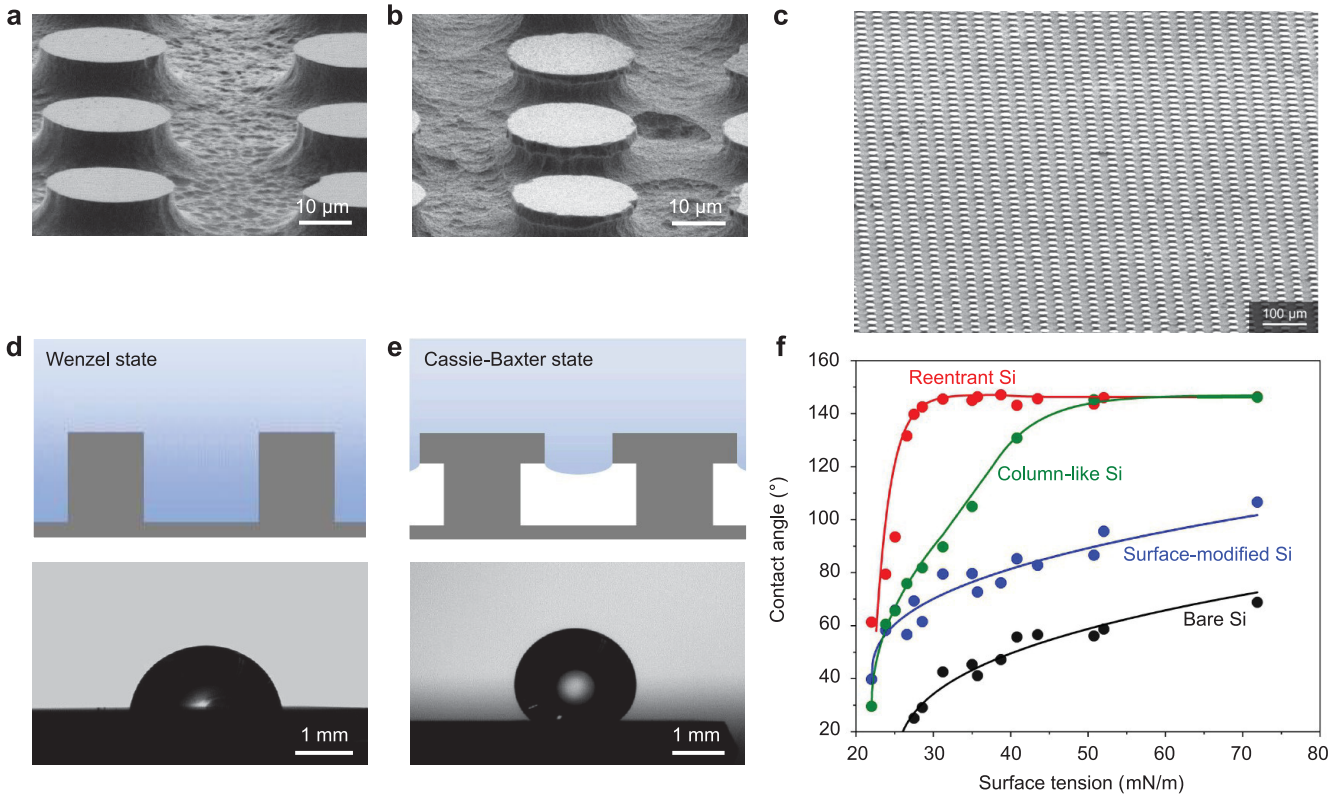

Figure 5. Fabrication of 3D structures for the omniphobic silicon surface. (a, b) SEM images of fabricated arrays of 3D microstructures: (a) simple column-like structures and (b) reentrant structures. (c) SEM image for a large-scale array of reentrant structures. (d, e) Contact angles observed on surfaces with (d) simple and (e) reentrant structures when the 50% water−ethanol mixture whose surface tension is 28.57 mN/m was dropped on the surface. (f) Apparent contact angles depending on surface tensions of dropped liquids.

hard to fabricate with conventional rigid and thick mask materials are achievable.

In Figure 4, we explore how to modulate the etch rate by changing the feature size to create 3D structures with different heights. To further investigate the etching behavior of XeF_2 gas beyond the characteristics shown in Figures 2c and S2, we fabricated line patterns with various widths in graphene etch masks supported by a PMMA layer. Subsequently, for each line width, we measured the lateral and vertical etch rates of the Si substrate when exposed to XeF_2 gas at 3 Torr for 200 s (Figure 4a). Figure 4b shows the resulting measured vertical and lateral etch rates versus width. For graphene etch masks with a hole width smaller than 5 μm, the vertical etch rate is strongly dependent on the hole size. Thus, by modulating the hole size, we can engineer 3D structures. To modulate the etching depth of the Si substrate, we fabricated arrays of square holes with varying sizes of 0.6, 1.4, 2, and 3.6 μm and the same pitch of 1.4 μm by e-beam lithography as illustrated in the graphene etch mask design of Figure 4c. As shown in Figure 4d, after XeF_2 etching, a step-like structure was achieved with the etching depth corresponding to the size of the holes. The etching depths measured by a surface profiler are approximately 4, 6, and 9 μm for hole sizes of 1.4, 2, and 3.6 μm, respectively. The Si substrate under the mask patterned with 0.6 μm sized holes was not fully etched due to a low lateral etch rate when compared to the pitch between each hole. As a result, the etching depth could not be measured by the surface profiler.

In Figures 4f,g and S7, we show the applicability of the graphene etch mask's deformability and controlling etch size to create complex 3D structures by selectively patterning regions with 2 μm square holes. Together with different etching depths, we can observe that the fabricated structures are wrapped in graphene. It is noteworthy that the step-like and graphene-wrapped 3D structures can be fabricated in a single-step etching process by employing a graphene etch mask. This is possible because graphene can effectively protect the substrate due to its deformable nature during etching. This stands in stark contrast to conventional etch masks, which lack such flexibility and deformability.

In Figure 5, we apply the deformable graphene etch masks to create double-reentrant structures and control surface wettability. Surface 3D microstructures have been used to control surface wettability.[32] Particularly, reentrant 3D structures are widely employed to achieve omniphobic surfaces.[33−35] However, the conventional methods for fabricating the reentrant structures tend to be complicated.[34,36] In this regard, the graphene etch mask can streamline the fabrication process for reentrant 3D structures. For comparison, we fabricated two samples on the Si substrates by using graphene etch masks, each consisting of an array of distinct 3D microstructures of the identical size scale: one with a column-like 3D structure (Figure 5a) and the other with a reentrant 3D structure (Figure 5b). A large-scale array of reentrant structures, sufficient for conducting contact angle measurements, was fabricated. (Figure 5c). After etching, the graphene etch mask was removed using CF_4 plasma, followed by surface modification to enhance the intrinsic hydrophobicity of Si.[37,38] The Si surface was coated with 1H,1H,2H,2H-perfluorooctyltrichlorosilane (PFOTS) for surface modifica-

https://doi.org/10.1021/acsnano.4c01279
ACS Nano XXXX, XXX, XXX−XXX

tion. Contact angles of the fabricated Si surfaces were measured by dropping droplets of a water−ethanol mixture (1:1; Figure 5d,e). On the column-like 3D structure, we observed the Wenzel state, where the liquid completely fills the gaps between pillars and contacts with the entire exposed surface of the solid. Conversely, we observed the Cassie−Baxter state on the surface with reentrant structures, in which the liquid does not infiltrate the gaps and makes contact with the interface consisting of both solid and vapor. This resulted in a superhydrophobic surface with a higher contact angle compared to the Wenzel state.

To examine the omniphobic characteristics of the fabricated reentrant structure, we utilized liquids with varying surface tensions. The surface energy of the water−ethanol mixture varies depending on the mixing ratio.[39] (See Figure S8 for the surface tension of the water−ethanol mixture used in this work.) As shown in Figure 5f, we measured the contact angles of the water−ethanol mixture on different substrates, including the bare Si substrate, surface-modified Si substrate, column-like 3D structure of Figure 5a, and reentrant 3D structure of Figure 5b. All 3D structures fabricated on Si substrates were also treated by PFOTS. Both column-like and reentrant Si surfaces showed significantly higher contact angles than the bare and surface-modified Si surfaces. Even though the Cassie−Baxter state with high contact angles of >140° is achieved in both 3D structures for liquids with high surface tension of >50 mN/m, the column-like Si cannot maintain the Cassie−Baxter state for liquids with a lower surface tension of <35 mN/m. In contrast, the reentrant structures consistently exhibited omniphobic characteristics, effectively repelling liquids with surface tensions exceeding 25 mN/m. Additionally, as shown in Figure S9, both surface-treated silicon and surface-treated graphene/silicon exhibit similar contact angles, indicating that the presence of graphene does not significantly influence the wettability of the surface. These findings underscore the capabilities of our Si-based reentrant structures in governing surface wettability across a broad spectrum of liquid types and surface tensions.

CONCLUSIONS

In conclusion, the advancement of 3D microfabrication through cutting-edge manufacturing technology is pivotal for enhancing the performance across various research fields. In this study, we developed a method to fabricate 3D microstructures by using an ultrathin and deformable graphene etch mask. The graphene directly synthesized on the Si substrate effectively serves as an efficient etch mask capable of generating intricate designs including mushroom-like structures. By incorporating a straightforward wrapping process with creatively designed graphene, we achieved the production of 3D structures that were previously challenging to manufacture by using conventional methods. Furthermore, our entire process, from graphene synthesis to wrapping, is scalable to a wafer scale. We successfully fabricated arrays of reentrant structures showing omniphobic surfaces on Si substrates. Beyond its ability to control surface wettability, our graphene-based etching technique can be applied to a wide range of lithographic applications. Our work contributes to the ongoing developments in diverse fields related to 3D microfabrication.

METHODS

Direct Graphene Growth on Si Wafer. Graphene was synthesized on the Si substrates by the APCVD method. First, the Si substrate was positioned within a 2 in. diameter quartz tube and heated up to 1020 °C for 1 h under H_2 (100 sccm). At 1020 °C, CH_4 gas (25 sccm) and H_2 (100 sccm) were supplied for 2 h at atmospheric pressure. After the growth, all gas flow was turned off and the chamber was rapidly cooled to room temperature by pumping to low pressure.

Characterization of Synthesized Graphene. To characterize the synthesized graphene, Raman spectroscopy with a 532 nm laser (Horiba, LabRAM HR Evolution) was used. We used AFM (Park System NX-10) for imaging and thickness measurements. We used cs-corrected monochromated TEM (Thermo Fisher, Themis Z) at an acceleration voltage of 80 kV for SAED, HRTEM, and DF-TEM images.

Fabrication of 3D Structures with a Graphene Mask. To pattern the grown graphene, an e-beam resist (950 PMMA A6) or photoresist (AZ5214E) was coated, followed by e-beam lithography (TESCAN, MIRA3 XMH) or photolithography (The Heidelberg MLA 150 Maskless Aligner). To pattern the graphene mask, the reactive ion etching (RIE) system (Samco, RIE-10NR) was used with a CF_4 flow rate of 20 sccm and a power of 30 W for 3 min. Samples were immersed in acetone for 10 min to remove the e-beam resist or photoresist and rinsed by IPA. A XeF_2 etching system (SAMCO, VPE-4F) was employed to etch the Si substrate at P_{XeF_2} = 3 Torr, $t_{exposure}$ = 2−5 min, and room temperature (≈20 °C). Exposure time to XeF_2 was varied to achieve the desired etching depth.

Wrapping Process of the Graphene Mask. To wrap around the underlying silicon structure with the suspended graphene mask, IPA was directly dropped onto the sample. After the sample surface dried in the air, this dropping and drying process was repeated (a total of 2−3 times) to ensure the proper wrapping of graphene. Subsequently, additional etching can be performed to fabricate 3D structures, including mushroom-like structures.

Characterization of Fabricated 3D Microstructures. Scanning electron microscopy (SEM, SUPRA 55VP) was used to observe the fabricated 3D structures in the Secondary Electron Detector (SE2) mode at an operating voltage of 2−10 kV. The surface profile of the etched Si surface was measured by a surface profiler (Bruker, DektakXT-A).

Fabrication of Omniphobic Surfaces and Measurement of Contact Angles. After fabricating arrays of 3D structures, the graphene mask was removed by CF_4 plasma with a CF_4 flow rate of 20 sccm and a power of 30 W for 3 min. 1H,1H,2H,2H-Perfluorooctyltrichlorosilane (PFOTS, 97%, Sigma-Aldrich) was used for surface modification. Samples were immersed in chloroform with a few drops of PFOTS for 4 h. Contact angles were measured using a contact angle goniometer (The Ramé-Hart, model 250) at room temperature.

ASSOCIATED CONTENT

Supporting Information

The Supporting Information is available free of charge at https://pubs.acs.org/doi/10.1021/acsnano.4c01279.

APCVD graphene growth for the graphene etch mask (Figure S1); etching characteristics of the Si substrate with a rectangular patterned graphene mask when exposed to XeF_2 (Figure S2); 3D graphene/silicon suspended structures (Figure S3); deformability of exfoliated graphene depending on thickness (Figure S4); deformability of CVD-grown graphene depending on thickness (Figure S5); controlling the shapes of upper protruding parts in fabricated 3D reentrant structures (Figure S6); fabrication of complex 3D structures with the deformable graphene mask (Figure S7); surface tension of ethanol/water mixtures (Figure S8); and the influence of graphene on the wettability of the surface (Figure S9) (PDF)

https://doi.org/10.1021/acsnano.4c01279
ACS Nano XXXX, XXX, XXX−XXX

AUTHOR INFORMATION

Corresponding Author

Gwan-Hyoung Lee − *Department of Materials Science and Engineering, Seoul National University, Seoul 08826, South Korea;* orcid.org/0000-0002-3028-867X; Email: gwanlee@snu.ac.kr

Authors

Jiwoo Kim − *Department of Materials Science and Engineering, Seoul National University, Seoul 08826, South Korea;* orcid.org/0009-0008-7462-8593

Donghoon Moon − *Department of Materials Science and Engineering, Seoul National University, Seoul 08826, South Korea;* orcid.org/0009-0009-6314-235X

Hyunchul Kim − *Department of Mechanical Science and Engineering, University of Illinois Urbana-Champaign (UIUC), Urbana, Illinois 61801, United States;* orcid.org/0000-0002-6883-6985

Arend M. van der Zande − *Department of Mechanical Science and Engineering, University of Illinois Urbana-Champaign (UIUC), Urbana, Illinois 61801, United States;* orcid.org/0000-0001-5104-9646

Complete contact information is available at: https://pubs.acs.org/10.1021/acsnano.4c01279

Notes

The authors declare no competing financial interest.

ACKNOWLEDGMENTS

This work was supported by Basic Science Research Program (NRF-2021R1A2C3014316) through the National Research Foundation of Korea (NRF) funded by the Ministry of Science, ICT & Future Planning and by the Technology Innovation Program (RS-2023-00301731) funded by the Ministry of Trade, Industry & Energy (MOTIE). G.-H.L. acknowledges the support from the Research Institute of Advanced Materials (RIAM), Institute of Engineering Research (IER), Institute of Applied Physics (IAP), and Inter-University Semiconductor Research Center (ISRC) at the Seoul National University. This work was supported by supported by the NSF through the University of Illinois at Urbana-Champaign Materials Research Science and Engineering Center under Award Number DMR-1720633 and DMR-2309037. This work was carried out in part in the Holonyak Micro and Nano Technology Laboratory (HMNTL) and the Materials Research Laboratory Central Facilities (MRL), at the University of Illinois Urbana-Champaign. The authors acknowledge the use of facilities and instrumentation supported by NSF through the University of Illinois Materials Research Science and Engineering Center DMR-2309037.

REFERENCES

(1) Hassanin, H.; Sheikholeslami, G.; Sareh, P.; Ishaq, R. B. Microadditive manufacturing technologies of 3D microelectromechanical systems. *Adv. Eng. Mater.* **2021**, *23* (12), No. 2100422.

(2) Fan, X.; Smith, A. D.; Forsberg, F.; Wagner, S.; Schroder, S.; Akbari, S. S. A.; Fischer, A. C.; Villanueva, L. G.; Ostling, M.; Lemme, M. C.; Niklaus, F. Manufacture and characterization of graphene membranes with suspended silicon proof masses for MEMS and NEMS applications. *Microsyst. Nanoeng.* **2020**, *6*, 17.

(3) Ho, C. M. B.; Mishra, A.; Hu, K.; An, J.; Kim, Y. J.; Yoon, Y. J. Femtosecond-laser-based 3D printing for tissue engineering and cell biology applications. *ACS Biomater. Sci. Eng.* **2017**, *3* (10), 2198−2214.

(4) Liu, L. W. Y.; Virdee, B. S.; Inal, J.; Steer, M. B. Microfabrication of conical microfunnels for drug delivery applications. *Micro−Nano Lett.* **2015**, *10* (7), 355−357.

(5) Chircov, C.; Grumezescu, A. M. Microelectromechanical systems (MEMS) for biomedical applications. *Micromachines* **2022**, *13* (2), No. 164.

(6) Guo, X.; Xue, Z.; Zhang, Y. Manufacturing of 3D multifunctional microelectronic devices: challenges and opportunities. *NPG Asia Mater.* **2019**, *11* (1), No. 29.

(7) Huang, Y.; Wu, X.; Liu, H.; Jiang, H. Fabrication of through-wafer 3D microfluidics in silicon carbide using femtosecond laser. *J. Micromech. Microeng.* **2017**, *27* (6), No. 065005.

(8) Ren, Z.; Chang, Y.; Ma, Y.; Shih, K.; Dong, B.; Lee, C. Leveraging of MEMS technologies for optical metamaterials applications. *Adv. Opt. Mater.* **2019**, *8* (3), No. 1900653.

(9) Chen, S.; Liu, Z.; Du, H.; Tang, C.; Ji, C. Y.; Quan, B.; Pan, R.; Yang, L.; Li, X.; Gu, C.; et al. Electromechanically reconfigurable optical nano-kirigami. *Nat. Commun.* **2021**, *12* (1), No. 1299.

(10) Sakellari, I.; Yin, X.; Nesterov, M. L.; Terzaki, K.; Xomalis, A.; Farsari, M. 3D chiral plasmonic metamaterials fabricated by direct laser writing: the twisted omega particle. *Adv. Opt. Mater.* **2017**, *5* (16), No. 1700200.

(11) Gil-Santos, E.; Baker, C.; Lemaitre, A.; Ducci, S.; Gomez, C.; Gomez, C.; Leo, G.; Leo, G.; Favero, I. Scalable high-precision tuning of photonic resonators by resonant cavity-enhanced photoelectrochemical etching. *Nat. Commun.* **2017**, *8*, No. 14267.

(12) Han, E.; Yu, J.; Annevelink, E.; Son, J.; Kang, D. A.; Watanabe, K.; Taniguchi, T.; Ertekin, E.; Huang, P. Y.; van der Zande, A. M. Ultrasoft slip-mediated bending in few-layer graphene. *Nat. Mater.* **2020**, *19* (3), 305−309.

(13) Lee, C.; Wei, X.; Kysar, J. W.; Hone, J. Measurement of the elastic properties and intrinsic strength of monolayer graphene. *Science* **2008**, *321* (5887), 385−388.

(14) Lee, G.-H.; Cooper, R. C.; An, S. J.; Lee, S.; van der Zande, A.; Petrone, N.; Hammerberg, A. G.; Lee, C.; Crawford, B.; Oliver, W.; et al. High-strength chemical-vapor−deposited graphene and grain boundaries. *Science* **2013**, *340* (6136), 1073−1076.

(15) Bae, S.; Kim, H.; Lee, Y.; Xu, X.; Park, J.-S.; Zheng, Y.; Balakrishnan, J.; Lei, T.; Kim, H. R.; Song, Y. I.; et al. Roll-to-roll production of 30-in. graphene films for transparent electrodes. *Nat. Nanotechnol.* **2010**, *5* (8), 574−578.

(16) Miao, J.; Fan, T. Flexible and stretchable transparent conductive graphene-based electrodes for emerging wearable electronics. *Carbon* **2023**, *202*, 495−527.

(17) Bunch, J. S.; Verbridge, S. S.; Alden, J. S.; van der Zande, A. M.; Parpia, J. M.; Craighead, H. G.; McEuen, P. L. Impermeable atomic membranes from graphene sheets. *Nano Lett.* **2008**, *8* (8), 2458−2462.

(18) Berry, V. Impermeability of graphene and its applications. *Carbon* **2013**, *62*, 1−10.

(19) Kim, S. W.; Seol, M.; Cho, Y.; Shin, K. W.; Lee, D.; Jeong, S.-J.; Lee, H.; Chung, J. G.; Kim, H.-M.; Kim, K.-B.; et al. Graphene-based etch resist for semiconductor device fabrication. *ACS Appl. Nano Mater.* **2020**, *3* (5), 4635−4641.

(20) Radovic, L. R.; Bockrath, B. On the chemical nature of graphene edges: origin of stability and potential for magnetism in carbon materials. *J. Am. Chem. Soc.* **2005**, *127* (16), 5917−5927.

(21) Xu, D.; Xiong, B.; Wu, G.; Wang, Y.; Sun, X.; Wang, Y. Isotropic silicon etching with XeF_2 gas for wafer-level micromachining applications. *J. Microelectromech. Syst.* **2012**, *21* (6), 1436−1444.

(22) Stine, R.; Lee, W. K.; Whitener, K. E., Jr.; Robinson, J. T.; Sheehan, P. E. Chemical stability of graphene fluoride produced by exposure to XeF_2. *Nano Lett.* **2013**, *13* (9), 4311−4316.

(23) Liu, Y.; Noffke, B. W.; Qiao, X.; Li, Q.; Gao, X.; Raghavachari, K.; Li, L. S. Basal plane fluorination of graphene by XeF_2 via a radical cation mechanism. *J. Phys. Chem. Lett.* **2015**, *6* (18), 3645−3649.

(24) Son, J.; Ryu, H.; Kwon, J.; Huang, S.; Yu, J.; Xu, J.; Watanabe, K.; Taniguchi, T.; Ji, E.; Lee, S.; et al. Tailoring single- and double-Sided fluorination of bilayer graphene via substrate interactions. *Nano Lett.* **2021**, *21* (2), 891−898.
(25) Feng, W.; Long, P.; Feng, Y.; Li, Y. Two-dimensional fluorinated graphene: synthesis, structures, properties and applications. *Adv. Sci.* **2016**, *3* (7), No. 1500413.
(26) Fang, C.; Shapter, J. G.; Voelcker, N. H.; Ellis, A. V. Graphene masks as passivation layers in the electrochemical etching of silicon. *J. Mater. Sci.* **2014**, *49* (22), 7819−7823.
(27) Son, J.; Kwon, J.; Kim, S.; Lv, Y.; Yu, J.; Lee, J.-Y.; Ryu, H.; Watanabe, K.; Taniguchi, T.; Garrido-Menacho, R.; et al. Atomically precise graphene etch stops for three dimensional integrated systems from two dimensional material heterostructures. *Nat. Commun.* **2018**, *9* (1), No. 3988.
(28) Khan, A.; Habib, M. R.; Jingkun, C.; Xu, M.; Yang, D.; Yu, X. New insight into the metal-catalyst-free direct chemical vapor deposition growth of graphene on silicon substrates. *J. Phys. Chem. C* **2021**, *125* (3), 1774−1783.
(29) Eckmann, A.; Felten, A.; Mishchenko, A.; Britnell, L.; Krupke, R.; Novoselov, K. S.; Casiraghi, C. Probing the nature of defects in graphene by Raman spectroscopy. *Nano Lett.* **2012**, *12* (8), 3925−3930.
(30) Huang, P. Y.; Meyer, J. C.; Muller, D. A. From atoms to grains: transmission electron microscopy of graphene. *MRS Bull.* **2012**, *37* (12), 1214−1221.
(31) Kim, K.; Lee, Z.; Regan, W.; Kisielowski, C.; Crommie, M. F.; Zettl, A. Grain boundary mapping in polycrystalline graphene. *ACS Nano* **2011**, *5* (3), 2142−2146.
(32) Wang, F.; Wu, Y.; Nestler, B. Wetting effect on patterned substrates. *Adv. Mater.* **2023**, *35* (25), No. 2210745.
(33) Li, J.; Han, X.; Li, W.; Yang, L.; Li, X.; Wang, L. Nature-inspired reentrant surfaces. *Prog. Mater. Sci.* **2023**, *133*, No. 101064.
(34) Liu, T. L.; Kim, C.-J. C. Turning a surface superrepellent even to completely wetting liquids. *Science* **2014**, *346* (6213), 1096−1100.
(35) Wang, W.; Zhang, Y.; Chen, T.; Sun, X.; Mei, X.; Cui, J. Wettability and stability of wetting states for the surfaces with reentrant structures. *J. Phys. Chem. C* **2020**, *124* (52), 28479−28487.
(36) Liu, X.; Gu, H.; Wang, M.; Du, X.; Gao, B.; Elbaz, A.; Sun, L.; Liao, J.; Xiao, P.; Gu, Z. 3D Printing of bioinspired liquid superrepellent structures. *Adv. Mater.* **2018**, *30* (22), No. 1800103.
(37) Afonso, E.; Martínez-Gómez, A.; Huerta, A.; Tiemblo, P.; García, N. Facile preparation of hydrophobic PET surfaces by solvent induced crystallization. *Coatings* **2022**, *12* (2), No. 137.
(38) Sriram, S.; Singh, R. K.; Kumar, A. Silica and silane based polymer composite coating on glass slide by dip-coating method. *Surf. Interfaces* **2020**, *19*, No. 100472.
(39) Phan, C. M. The surface tension and interfacial composition of water/ethanol mixture. *J. Mol. Liq.* **2021**, *342*, No. 117505.

https://doi.org/10.1021/acsnano.4c01279
ACS Nano XXXX, XXX, XXX−XXX